Transients and the Extratropical Response to El Niño

ISAAC M. HELD

Geophysical Fluid Dynamics Laboratory, Princeton University, Princeton, New Jersey

STEVEN W. LYONS

Department of Meteorology Texas A & M University, College Station, Texas

SUMANT NIGAM

Center for the Study of Ocean–Land–Atmosphere Interactions, Department of Meteorology, University of Maryland, College Park, Maryland

(Manuscript received 11 April 1988, in final form 2 August 1988)

ABSTRACT

A baroclinic stationary wave model linearized about a zonally symmetric flow is used to interpret the extratropical atmospheric response to El Niño produced by a general circulation model. When forced by the anomalous diabatic heating and tendency due to transients, the linear model provides a useful simulation of this response. The direct response to anomalous diabatic heating is found to be small in the extratropics; the dominant term is the response to the anomalous transients, particularly the anomalous upper tropospheric transients in the vorticity equation. These results are complementary to those obtained with a nonlinear barotropic model by Held and Kang, and indicate that the anomalous subtropical convergence which plays a key role in that study is itself primarily forced by the anomalous transients. One can distinguish between two distinct parts of the response of the transients to the tropical heating: the movement of the Pacific storm track associated with the anomalous extratropical wave train, and changes in the penetration of Rossby waves into the tropics resulting from the modified tropical winds.

1. Introduction

In Held and Kang (1987, hereafter referred to as HK), barotropic models are used to help interpret the extratropical response to El Niño in a general circulation model (GCM). The GCM data are taken from a 15 yr integration studied by Lau (1985) in which climatological sea surface temperatures are imposed everywhere except in the equatorial Pacific, where the ocean temperatures, as observed in the period 1962–76, are specified. The GCM's circulation is composited over three El Niño and three anti-El Niño winters. The difference between the El Niño and anti-El Niño composites for the 300 mb geopotential (with the zonal mean removed) is reproduced in Fig. 1a. It is the dynamics of this anomaly, particularly the wave train spanning the North Pacific and North America, with which HK and the present paper are concerned. For a discussion of different theories for this extratropical wave train, see HK and the references therein. For discussion of the GCM integrations, see Lau (1985).

Corresponding author address: Dr. Isaac M. Held, Geophysical Fluid Dynamics Laboratory, Princeton University, Princeton, NJ 08542.

In HK the zonally averaged flow, the divergence anomaly, and the anomaly in the vorticity tendency due to transients at 300 mb are taken from the GCM, and barotropic models are used to diagnose the anomalous stationary eddy streamfunction at this level. A model linearized about the zonally asymmetric climatological flow, as in Simmons et al. (1983) and Branstator (1985), is found to reproduce the GCM as well as a fully nonlinear model, and the response can therefore be decomposed into elements forced by different parts of the anomalous divergence and transients. It is found that the forcing in the central Pacific is of greater importance than that in the western Pacific, that the response to the central Pacific forcing is not primarily due to the equatorial divergence associated with the increased rainfall near the dateline, but rather the convergence associated with compensating subsidence in the subtropics, and that the direct response to anomalous transients, though important in some regions, is generally not as large as the response to the subtropical divergence.

The result that the subtropical rather than tropical divergence field can be thought of as forcing the wave train in such a barotropic model is a serious complication. While the tropical divergence field can be con-

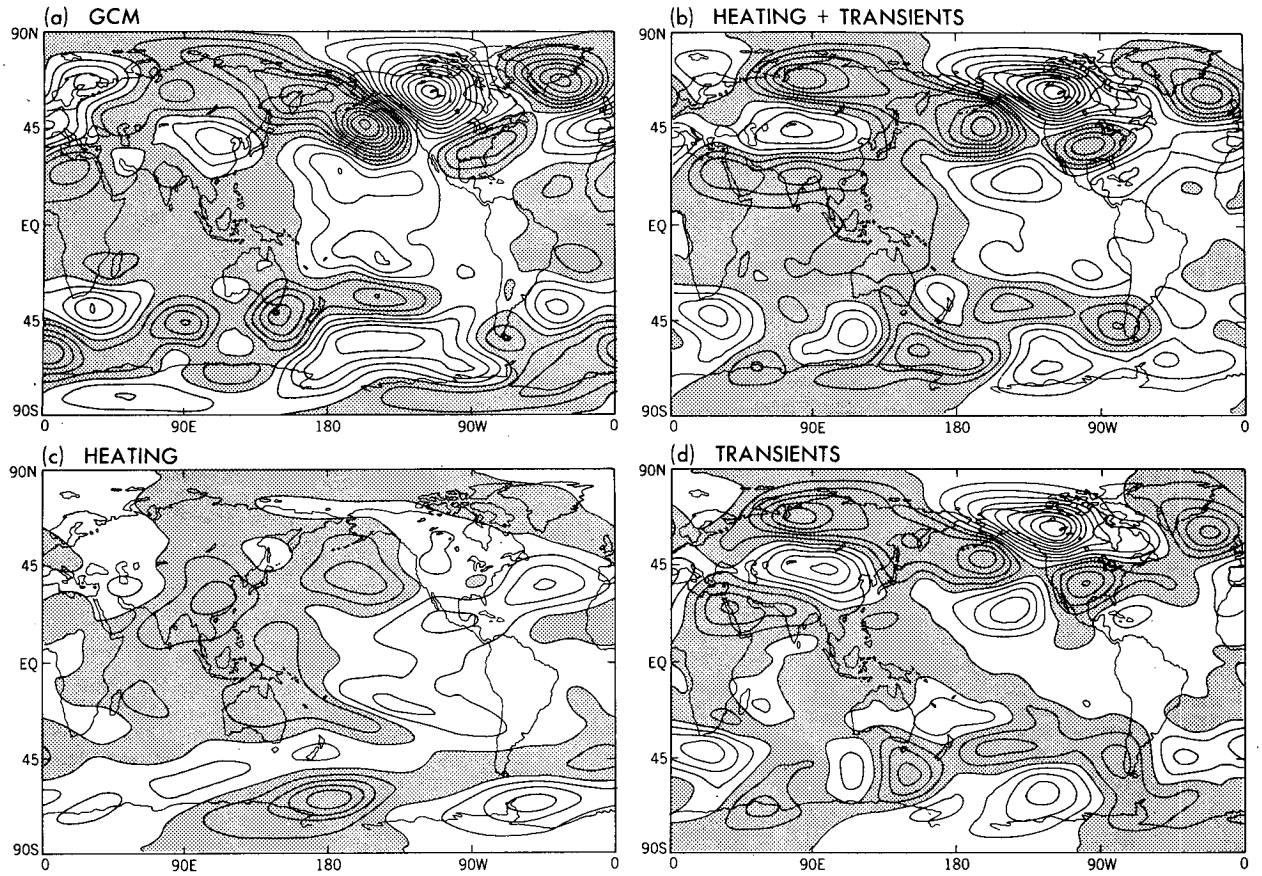

FIG. 1. (a) The 300 mb eddy geopotential height obtained from the GCM integration in Lau (1985) by compositing three El Niño winters and subtracting an analogous composite for three anti-El Niño winters; (b) the linear response of the 300 mb geopotential to the anomalous diabatic heating and forcing by transient eddies; (c) the linear response to anomalous diabatic heating; (d) the linear response to the anomalous forcing by transients. The contour interval is 10 m. Negative values are shaded.

sidered a direct consequence of the latent heating distribution, since the tropical thermodynamic equation reduces to a balance between diabatic heating and $-\omega\partial\Theta/\partial p$, this is not true in the subtropics, where horizontal temperature advection is also important. The anomalous subsidence in the subtropical central Pacific could be directly forced by the tropical latent heating anomaly, through linear wave propagation or nonlinear mechanisms; or it could be induced by anomalous transients which in turn are somehow forced by the tropical heating. In the latter case, the direct response to the anomalous transients in the barotropic model would not be a good measure of the total effect of transients on the response. A baroclinic model is needed to choose between these alternatives.

Nigam et al. (1986, 1988) (NHL1 and NHL2, respectively) describe a σ-coordinate, primitive equation, linear stationary wave model and its simulation of the wintertime, climatological waves produced by two GCMs: one with a flat lower boundary but with realistic continental distribution, and another with realistic orography. The model is linearized about the GCM's *zonally averaged* flow, and forced with the GCM's orography, diabatic heating field, and transient eddy heat and momentum fluxes. The linear model has precisely the same vertical levels and finite differencing as the GCM; however, it is finite-differenced in latitude, unlike the spectral GCM, and has higher meridional resolution (100 points from pole to pole). The linear model includes a Rayleigh friction that is large only near the surface and at those points at which the basic state zonal flow is weak. The functional form of this damping can be found in NHL1. One must expect the response to tropical heating to show some sensitivity to this Rayleigh friction. A description of the linear model is included in the Appendix.

We are encouraged to use this model to study the extratropical response to El Niño by the fact that it provides a reasonable simulation of the total upper tropospheric stationary wave field, as demonstrated in NHL2. The extratropical response to tropical forcing (Figs. 8 and 9 in NHL2) is a small part of the total

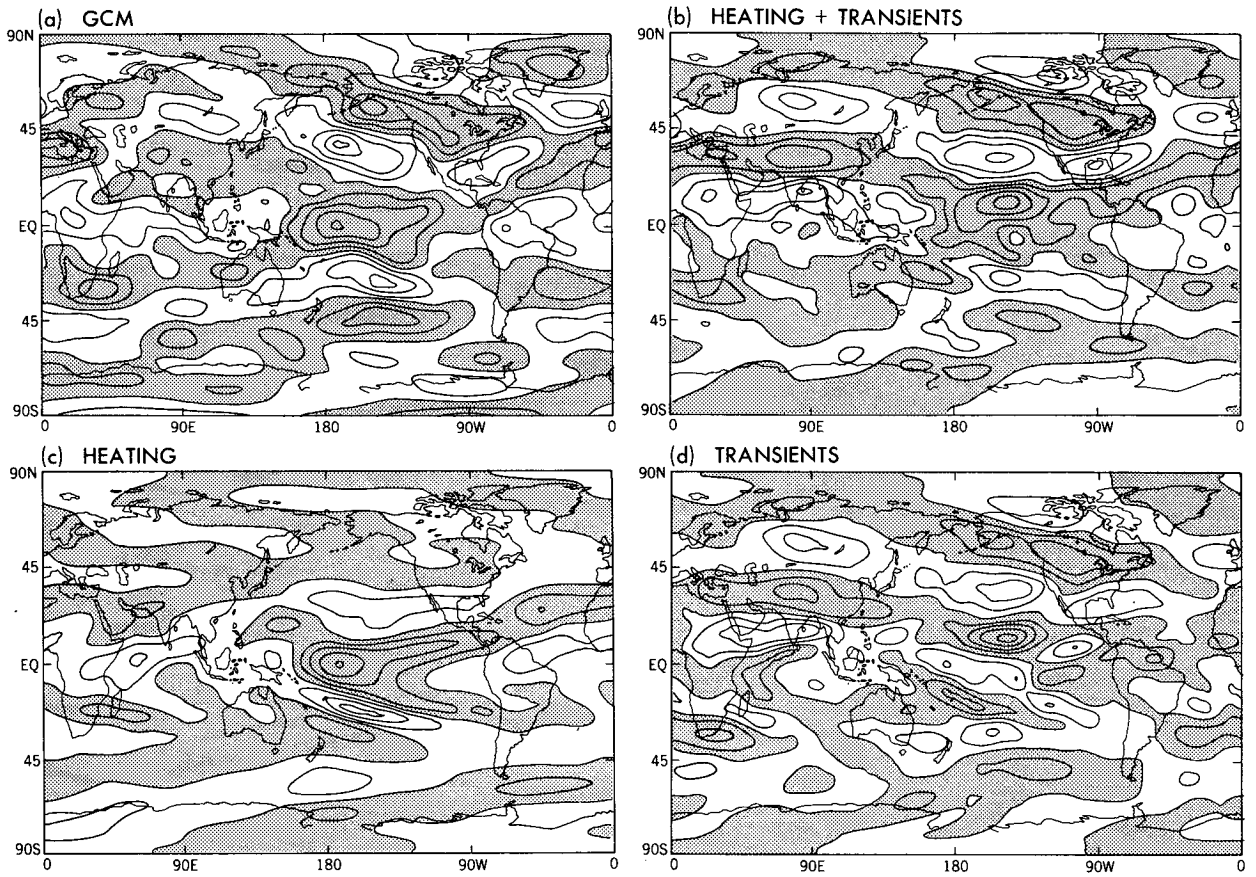

FIG. 2. As in Fig. 1, except for the eddy zonal wind at 300 mb. The contour interval is 2 m s^{-1}. Negative values are shaded.

eddy field, reaching amplitudes of only 50 gpm at 300 mb. This is much smaller than the contribution of midlatitude forcing, particularly orography, and it is difficult to judge whether or not the linear model is adequate for studying the stationary extratropical response to tropical heating.

The comparison in NHL1 is simpler in this regard, since orographic forcing is absent. The extratropical linear response to tropical forcing in that case is even weaker than in NHL2, but the total linear simulation is also weaker than the GCM's stationary wave field by 25%–30%, leaving open the possibility that the tropically forced portion of the wave field is being underpredicted. While there is some sensitivity to the form and strength of the friction imposed to remove the critical latitude singularity, as described in NHL1 and 2, we are unable to increase the amplitude of the extratropical response to tropical heating substantially in this linear model by modifying the frictional parameterization.

In the barotropic study of HK, a model linearized about a zonally symmetric flow does not provide as good a simulation of the extratropical wave train as does a model linearized about the climatological asymmetric flow. In particular, a model linearized about a zonal flow underestimates the importance of forcing in the western Pacific. This is consistent with the importance placed by Simmons et al. (1983) and Branstator (1985) on the interaction between the climatological stationary eddies and the disturbance forced by Indonesian heating. Since our baroclinic model is linearized about a zonally symmetric flow, one is led to suspect that it may have some difficulty in simulating the extratropical response. In this regard, it may be fortunate that the anomalous divergence field in the western Pacific does not play as large a role as the anomaly in the central Pacific in forcing this wave train, since the barotropic model suggests that interactions between the tropically forced wave and the climatological stationary waves are of less importance for central than for western Pacific forcing (see Fig. 6 in HK). On the other hand, as discussed in the concluding section of HK, the importance of this interaction in a barotropic model may be a poor guide to its importance in a baroclinic model.

Because the extratropical response to *climatological*

tropical heating in this linear model is smaller than the anomaly in Fig. 1a, we can anticipate that the extratropical response of the linear model to the *redistribution* of heating during El Niño will be substantially smaller than the anomaly as well.

2. Results

The El Niño and anti-El Niño composites have slightly different zonally averaged basic states, but we find that this difference has a negligible effect on the linear responses. This implies, on the one hand, that the waves forced by heating and transient eddy fluxes are insensitive to this change in the basic state and, on the other hand, that the orographic component of the stationary wave field can be ignored entirely. The anomalous extratropical wave train cannot be explained by a modification of the orographically forced waves resulting from a change in the basic state. In all of the calculations described below, the basic state is chosen to be the average of the zonal means of the El Niño and anti-El Niño composites.

Figure 1b shows the total linear response of 300 mb geopotential to the difference in heating between the two composites (the "anomalous" heating) plus the anomalous transient eddy forcing in the momentum and temperature equations. (As in NHL1 and NHL2, the temperature, vorticity, and divergence tendencies due to transients are computed by substituting the time-mean fields into the GCM's full σ-coordinate equations and subtracting the tendencies due to nonconservative effects. This procedure is repeated for each winter in the integration and the results composited over the El Niño and anti-El Niño years). Figure 1a is the difference between the GCM composites that we are trying to simulate. Although there are significant differences in the detailed patterns, for example, over northern Asia and in the Southern Hemisphere, we see that the dominant wave train over the North Pacific and North America is captured rather well when both the anomalous heating and forcing by transients are included in the linear model. In Figs. 1c and 1d, this response is split into separate parts forced by the anomalous heating (1c) and anomalous forcing by transients (1d). As expected, the heating alone forces an extratropical wave train that is much smaller than that generated by the GCM, although it does tend to have the correct phase in the Pacific–North American sector. The response to the anomalous transients is clearly dominant.

A different view of the response, emphasizing tropical structure, is provided by Fig. 2, which shows the anomalous eddy zonal winds in the same format as in Fig. 1. The total linear response yields nearly the correct latitudinal width of the tropical easterly anomaly. Heating alone produces easterlies that do not penetrate far enough into the northern subtropics, and a subtropical acceleration that is weak and also displaced equatorward. The *strength* of the linear equatorial wind response is very sensitive to the friction included in the model, but the *width* of the response is not. The forcing by transients appears to be needed to extend the easterly anomaly further northwards as well as to generate the bulk of the acceleration of the midlatitude winds in the central Pacific.

We can decompose this response further and determine which part of the transient forcing predominates.

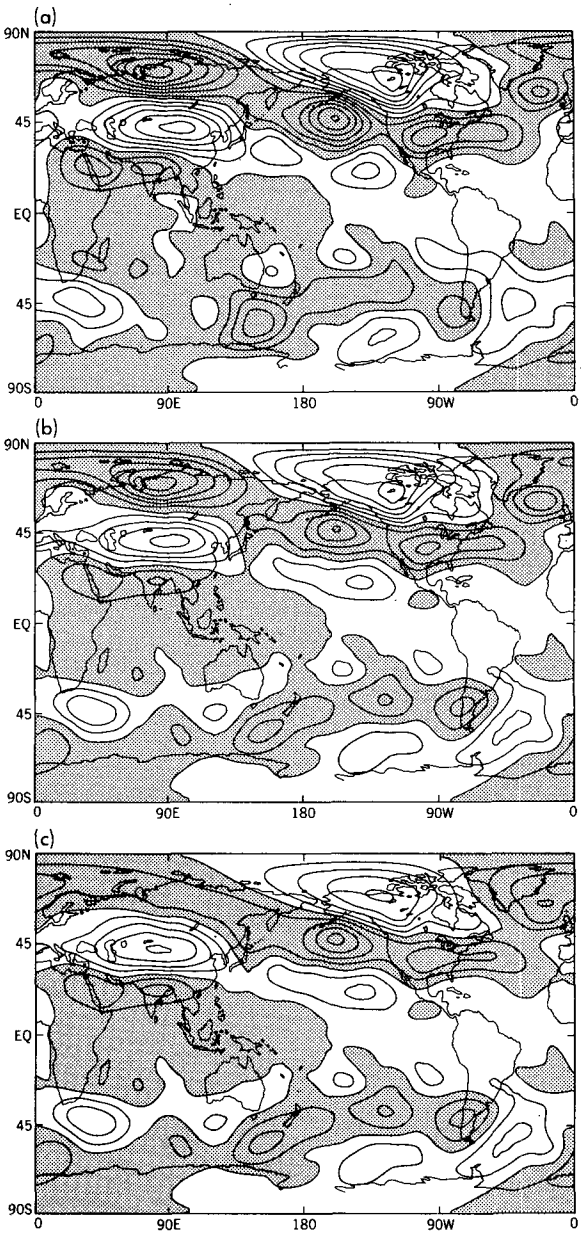

FIG. 3. The linear response of 300 mb geopotential height to (a) the anomalous vorticity tendency due to transients, (b) the anomalous vorticity tendency due to transients in the upper troposphere ($p < 600$ mb), and (c) the anomalous vorticity tendency due to transients in the upper troposphere, with high latitude forcing (>70°N) excluded. Contour interval is 10 m.

Figure 3a shows the 300 mb eddy geopotential produced by the anomalous transients in the vorticity equation, setting the forcing by transients in the temperature equation equal to zero. (The effect of transient forcing in the divergence equation is negligible.) These transients in the vorticity equation force most of the response in Fig. 1d. The effect of the thermal transients is largest over northern Canada, where they strengthen the anticyclonic anomaly. There is no tendency for the effects of anomalous thermal and vorticity transients to cancel. Decomposing into lower ($p > 600$ mb) and upper tropospheric vorticity transients, the latter is found to provide the bulk of the response. Figure 3b shows the response to the upper tropospheric vorticity transients. The largest change from Fig. 3a is a weakening of the low over the North Pacific. While still in good qualitative agreement with the GCM, after having subtracted out the direct response to heating, thermal transients, and lower tropospheric vorticity transients, the linear response in Fig. 3b is only half the amplitude of the GCM anomaly.

Experience with this linear model has shown us that, among other problems, it tends to distort the response to very high latitude forcing. Figure 3c is the response to upper tropospheric vorticity transients, analogous to Fig. 3b, except that the forcing north of 70°N has been removed. Although somewhat arbitrary, the result is to remove the anomalous low over northern Russia that is a significant source of disagreement between Figs. 1a and 1b. The response equatorwards of 45°N is not much affected. The forcing north of 70°N is set to zero in all of the linear model results to follow.

In the barotropic model of HK, in which the anomalous divergence is specified and the anomalous streamfunction computed, the extratropical wave train appears to be primarily forced by anomalous upper tropospheric convergence (i.e., subsidence) in the subtropical Pacific. For consistency with the present baroclinic diagnosis, we must assume that this subtropical subsidence is itself primarily forced by the anomalous transients. That this is the case is illustrated in Fig. 4, which shows the 300 mb velocity potential forced by the same anomalous upper tropospheric vorticity transients that generate Fig. 3c. The positive values in the subtropical North Pacific correspond to large-scale convergence and subsidence. Although the divergence fields are noisy, we have confirmed that a barotropic model, forced with the divergence that corresponds to the potential in Fig. 4, does produce a response very similar to that described in HK.

In Figs. 5a and 5b, the response in Fig. 3c is split into a part due to the anomalous forcing between 25° and 70°N and a part due to the forcing south of 25°N. (The contour interval has been reduced by a factor of 2 compared to the previous figures.) The midlatitude upper-tropospheric transients generate a wave train (5a) with considerable qualitative resemblance to the total response. Perhaps more surprisingly, the transients

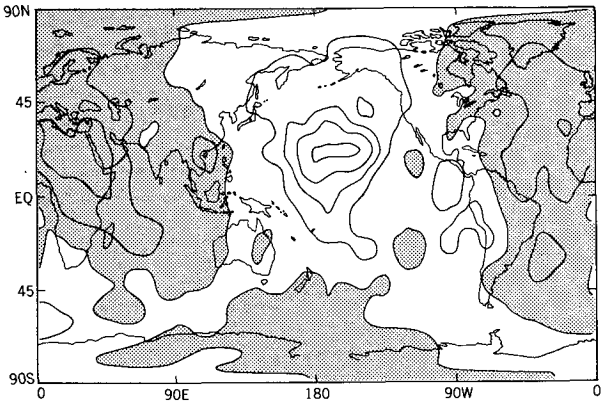

FIG. 4. The velocity potential at 300 mb produced by the linear response to the anomalous vorticity tendency due to transients in the upper troposphere. Contour interval is 5×10^5 m^2 s^{-1}. Negative values are shaded.

south of 25°N also generate a wave train (5b) of significant amplitude in the Northern Hemisphere. (Further decomposition shows that nearly all of this pattern is forced from the region north of the equator.) The response over Asia in Fig. 5, which can be traced through to the total linear response in Fig. 1b, is primarily forced from low latitudes. As described in section 3, the two parts of the response to anomalous transients in Figs. 5a and 5b appear to have distinct dynamical causes.

3. Transients

In order to analyze the transient forcing in more detail, it is useful to concentrate on one level in the atmosphere. To help motivate the choice of a level, we have decomposed the linear responses in Fig. 5 into parts generated by the anomalous vorticity forcing by transients at individual levels in the model. We find that most of the response to low-latitude forcing (5b) is generated from level 3 at $\sigma = 0.205$ (representing the layer from $\sigma = 0.28$ to 0.14). The response to midlatitude forcing (5a) is generated throughout the upper troposphere, but the horizontal structure of the midlatitude forcing does not change in any fundamental way with height. Thus, data near 200 mb should capture most of the relevant anomalous transient fluxes in the tropics and be representative of the midlatitude anomalous fluxes as well, although it will underestimate the quantitative importance of the midlatitude fluxes.

Figure 6a shows the response of the linear model to the anomalous vorticity tendency due to transients at σ-level 3 only. (The transient forcing is again obtained by computing the residual in the GCM's mean σ-coordinate vorticity equation.) Compared to the full response to anomalous transients, the response is quite naturally smaller (the contour interval is again one-half of that in Figs. 1–3) and is shifted eastward, con-

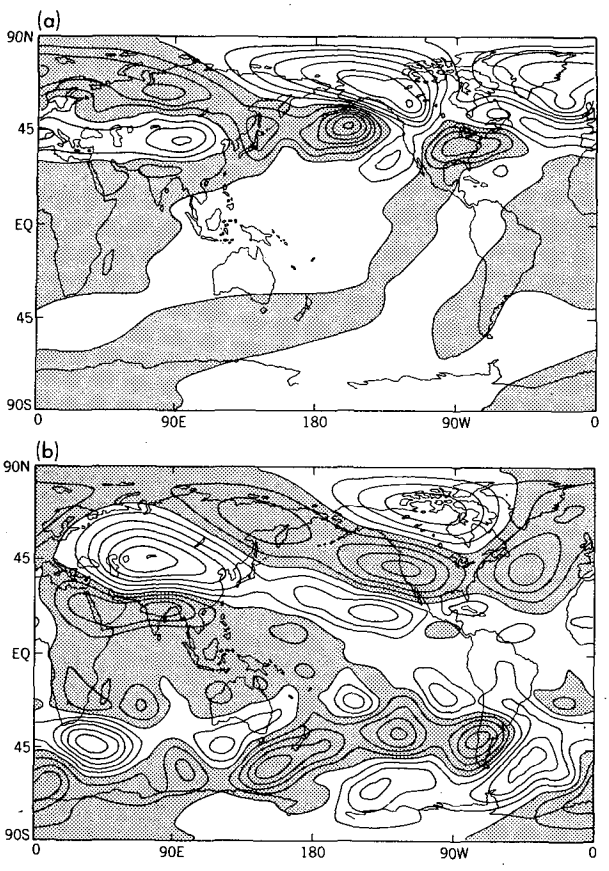

FIG. 5. The linear response of 300 mb geopotential height to the upper tropospheric anomalous vorticity tendency due to transients (a) between 25° and 70°N, and (b) south of 25°N. The contour interval is 5 m.

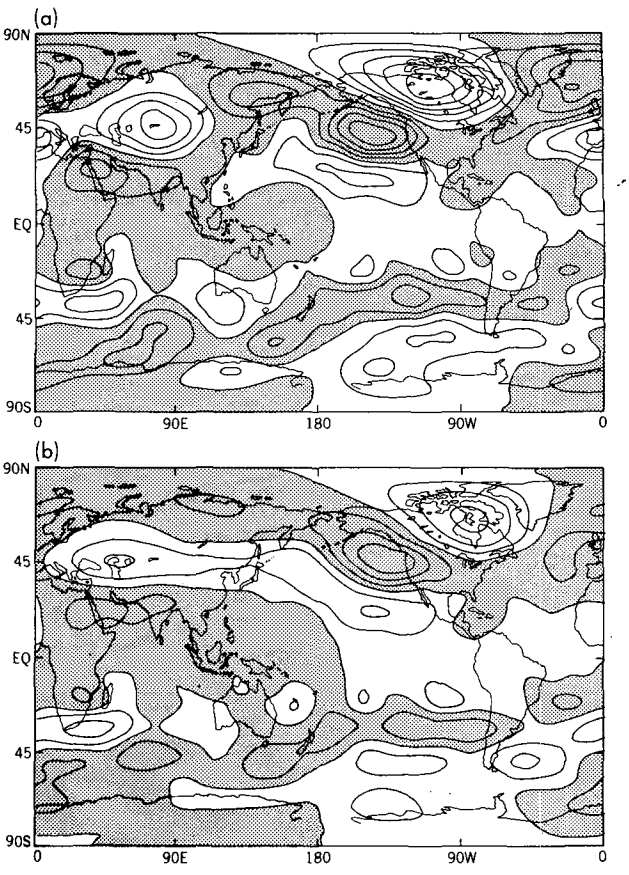

FIG. 6. The linear response of 300 mb geopotential height to the anomalous vorticity tendency due to transients near 200 mb, with the transient forcing computed in two different ways: (a) The vorticity tendency due to transients is computed as a residual from the GCM's seasonal mean σ-coordinate vorticity equation. (b) The difference between σ- and p-coordinate vorticity is ignored, and the anomalous transient eddy vorticity flux convergence at 200 mb, computed by sampling the GCM data once daily and interpolating to 200 mb, is substituted into the linear model at this same σ-level. Contour interval is 5 m.

sistent with the fact that a larger fraction of the response to low-latitude forcing is being captured at this level (cf. Fig. 5b). When we decompose Fig. 6a into the response to low- and midlatitude forcing, the low-latitude part is found to be much more dominant than in Fig. 5.

We have taken the GCM data, sampled daily and interpolated to 200 mb, and computed the convergence of the transient eddy vorticity flux, $\nabla \cdot (\overline{\mathbf{v}'\zeta'})$ in pressure coordinates. This quantity is calculated for each winter separately, and then composited over the El Niño and anti-El Niño cases. The difference between these two composites is used to force the linear model at σ-level 3. The result is shown in Fig. 6b. The pattern of the response is very similar to that in Fig. 6a, but the amplitude is smaller. The difference between these two figures must be due to the neglect of vertical advection and twisting in 6b, differences between σ- and p-coordinate vorticity, or interpolation and sampling errors.

Figure 7 is the anomalous streamfunction tendency,

$$-\nabla^{-2}[\nabla \cdot (\overline{\mathbf{v}'\zeta'})] \qquad (1)$$

obtained from the explicitly computed vorticity fluxes

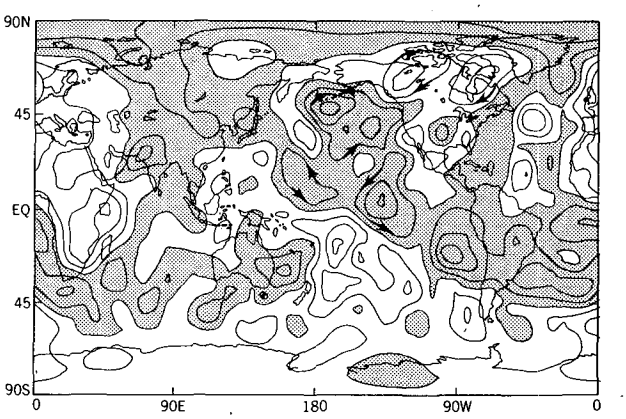

FIG. 7. The anomalous streamfunction tendency due to the 200 mb transients computed explicitly from the GCM data sampled daily and interpolated to 200 mb. Contour interval is 10 $m^2 s^{-2}$. Positive values are shaded.

that generate the response in Fig. 6b. (The vorticity tendency itself is too noisy to be easily interpreted.) There is an anomalous cyclonic tendency over much of the North Pacific and an anticyclonic tendency over northern Canada in the El Niño winters which, acting unopposed, would spin up streamfunction anomalies of the observed magnitude in 3 or 4 days. (However, a parcel of air passes through the center of anomalous cyclonic forcing over the North Pacific, for example, in less time than this, and, furthermore, the response is tempered by the induced vortex stretching.) There is also a distinct anomalous cyclonic tendency in low latitudes north of the equator over much of the Pacific. We have confirmed that the fluxes that produce this cyclonic tendency generate much of the response in the Pacific–North American sector in Fig. 6b, consistent with the fact that the low-latitude forcing dominates this picture. The anticyclonic tendency over Africa that penetrates into the Northern Hemisphere generates the response over North Africa and Asia in Fig. 6b.

[Figure 7 is substantially different from the streamfunction tendency due to transients displayed in HK (Fig. 1d) and used in their barotropic diagnosis of this same GCM integration. The difference is particularly pronounced in low latitudes. Nearly all of this difference is due to the fact that HK analyze the transients on the 300 mb rather than 200 mb surface. While the choice of level does not have a dramatic effect on the tendencies due to midlatitude eddies, the low latitutde flux anomalies are quite different at 200 and 300 mb.]

The difference in transient eddy activity between El Niño and anti–El Niño winters is most evident as a shift in the storm track in the eastern Pacific. Figure 8 is a plot of the variance of the 200 mb meridional velocity composited separately for the El Niño and anti-El Niño winters. Although all time scales from the daily sampling interval to the seasonal are retained, it is known that this field is dominated by high frequency "storm track" transients. In anti–El Niño years, the storm track in the eastern Pacific moves poleward into the Gulf of Alaska. In El Niño years, the latitude of the storm track is more nearly constant across the Pacific. We do not expect a low resolution model such as this to provide quantitatively correct storm tracks; however, this correlation between storm track location and the phase of the PNA pattern is qualitatively similar to that found in the atmosphere (e.g., Lau 1988). While this storm track movement must be responsible for the forcing of the anomalous stationary wave by midlatitude transients seen in Fig. 5a, it does not explain the low latitude forcing in Fig. 5b that dominates the response to the 200 mb transients.

If the horizontal flow is nondivergent, the eddy vorticity flux can be written in the form

$$\overline{v'\zeta'} = (a\mu^2)^{-1}[\partial_\lambda N - \partial_\theta(\mu M)], \qquad (2a)$$

$$\overline{u'\zeta'} = (a\mu^2)^{-1}[\partial_\lambda M + \partial_\theta(\mu N)], \qquad (2b)$$

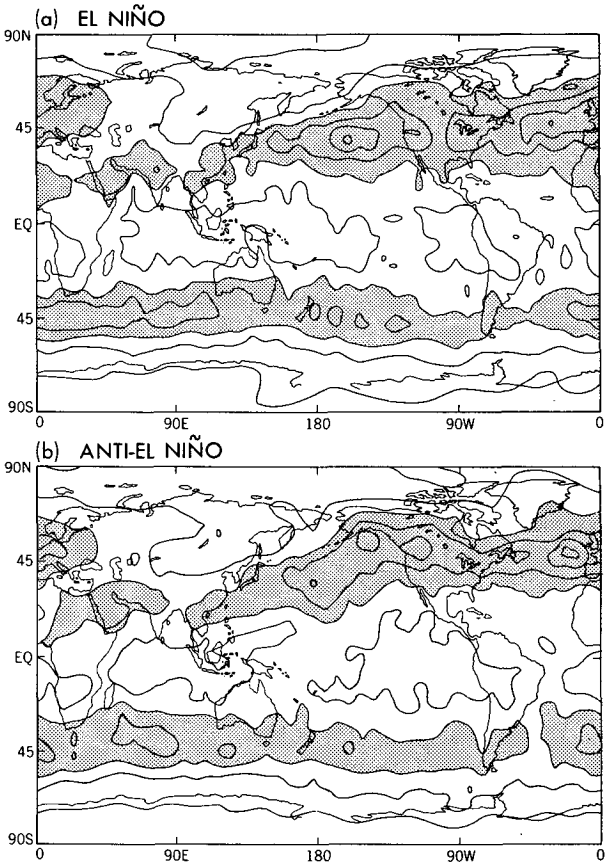

FIG. 8. The variance of the transient eddy meridional velocity, $\overline{v'^2}$, at 200 mb in the GCM analyzed by Lau (1985), composited separately for (a) El Niño and (b) anti–El Niño winters. Contour interval is 50 $m^2 s^{-2}$. Values greater than 150 $m^2 s^{-2}$ are shaded.

where

$$M = \mu\overline{u'v'},$$

and

$$N = \mu(\overline{v'^2} - \overline{u'^2})/2,$$

μ is the cosine of latitude and a the radius of the earth. Decomposing the streamfunction tendency (Fig. 7) and the linear response (Fig. 6b) into parts forced separately by $\overline{u'v'}$ and $(\overline{v'^2} - \overline{u'^2})/2$, we find the anomaly in $\overline{u'v'}$ to be, by far, the dominant term in both cases.

Figure 9 shows $\overline{u'v'}$ for the El Niño and anti–El Niño composites. In midlatitudes we see the change in orientation of the storm track clearly reflected in the momentum flux pattern, with convergence of westerly momentum into the eastern half of the Pacific storm track. The equatorward movement of the momentum convergence in the central and east Pacific in the El Niño composite can be thought of as enhancing the midlatitude westerly anomaly created by the tropical forcing and weakening the westerlies at higher latitudes.

There is also a significant difference between the *low* latitude momentum fluxes in the central Pacific: in the

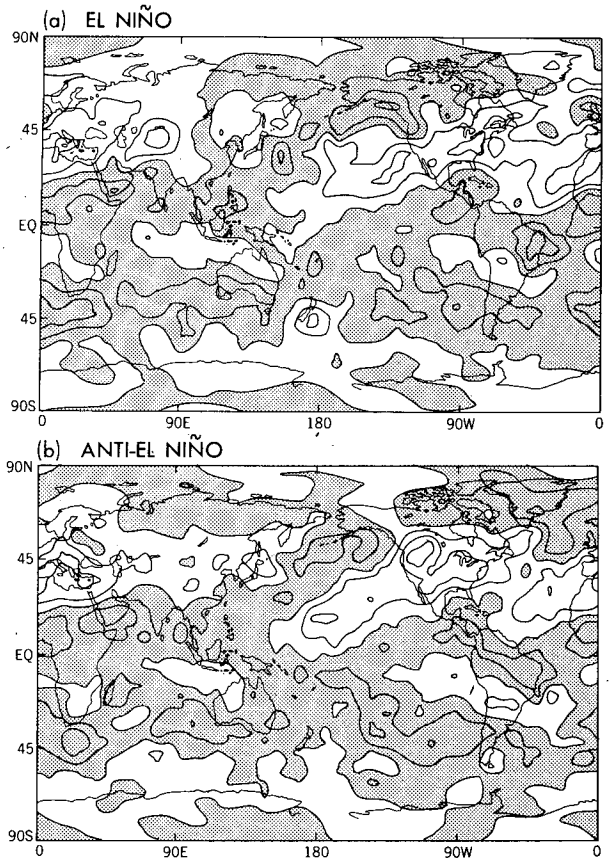

FIG. 9. As in Fig. 8, but for the eddy momentum flux, $\overline{u'v'}$. Contour interval is 20 $m^2 s^{-2}$. Negative values are shaded.

El Niño winters the momentum fluxes do not penetrate as far equatorward as in anti-El Niño winters. We presume that this is due to the 200 mb easterly anomaly along the equator in El Niño winters (Fig. 2a), which forces Rossby waves generated in midlatitudes to break and decelerate the zonal flow at a higher latitude than normal. The result is an anomalous easterly wind tendency at $\approx 15°$–$20°$N and a westerly tendency at lower latitudes, or, equivalently, the cyclonic tendency in low latitudes seen in Fig. 7. The redistribtuion of the low latitude deceleration of the zonal flow by Rossby waves results in a broadening of the tropical easterly anomaly in El Niño winters, which feeds back positively on the Rossby wave field and also generates the Northern Hemisphere extratropical response seen in Fig. 5b. While the amplitude of this wave train is modest, it is comparable to that of the wave train directly forced by the tropical heating anomaly.

To relate the momentum fluxes and eddy variances, it is informative to plot the vector field

$$\mathbf{E} = ([\overline{v'^2} - \overline{u'^2}]/2, -\overline{u'v'}).$$

If these barotropic statistics are dominated by Rossby waves with a definite frequency and local wavenumber, then **E** points in the direction of the corresponding group velocity (Hoskins et al. 1983; Plumb 1986). Figure 10 contains plots of **E** for the El Niño and anti-El Niño composites. The movement of the midlatitude storm track in the Pacific, in which $v'^2 > u'^2$, is clear, as is the deeper penetration of eddies into the tropical Pacific in the anti-El Niño winters. There are other interesting changes in eddy statistics as well. Over northern Africa, the structure of the transient eddies changes in a complex way from El Niño to anti-El Niño winters, and it is the associated momentum fluxes that force much of the pattern over Africa and Asia in the linear model.

An attempt was made to simulate anomalies in individual winters of the integration, and not simply the El Niño and anti-El Niño composites, but these were noticeably less successful. This suggests that there is a significant "free" component in individual seasonal means, and that the compositing does help isolate the response forced by the redistribution of latent heating in the tropics.

4. Conclusions

A baroclinic stationary wave model linearized about a zonally symmetric flow is found to provide a surprisingly good simulation of the difference in the extratropical stationary eddies between El Niño and anti-El Niño winters in the GCM integration analyzed by Lau (1985). In this case, at least, the interaction of the anomalous stationary wave and the climatological extratropical eddies, studied by Simmons et al. (1983) and Branstator (1985), does not appear to be of great importance. We suspect that this conclusion is not of general validity. There is little doubt that this interaction *can* play a role in the extratropical response to the redistribution of tropical heating, and a similar analysis of other integrations with this same GCM (M. Ting, personal communication) shows that models linearized about a zonally symmetric flow can fail badly. The barotropic results in Held and Kang (1987) suggest that a model linearized about a zonally symmetric flow may be adequate in this instance because it is the anomalous heating in the central rather than western Pacific that is dominant.

The linear simulation of this GCM response clearly demonstrates that the model's extratropical wave train is not simply the direct response to anomalous tropical heating; the response to the anomalous transients is vitally important, particularly the response to anomalies in the upper tropospheric vorticity fluxes. This result is consistent with the analysis by Kok and Opsteegh (1985) of the role of transients in the maintenance of the anomalous zonal winds over the Pacific in the El Niño of 1982–83. How these anomalies in the transient eddies are created by the tropical heating anomaly becomes a central problem in developing a theory for the extratropical wave train.

There seem to be two distinct ways in which upper

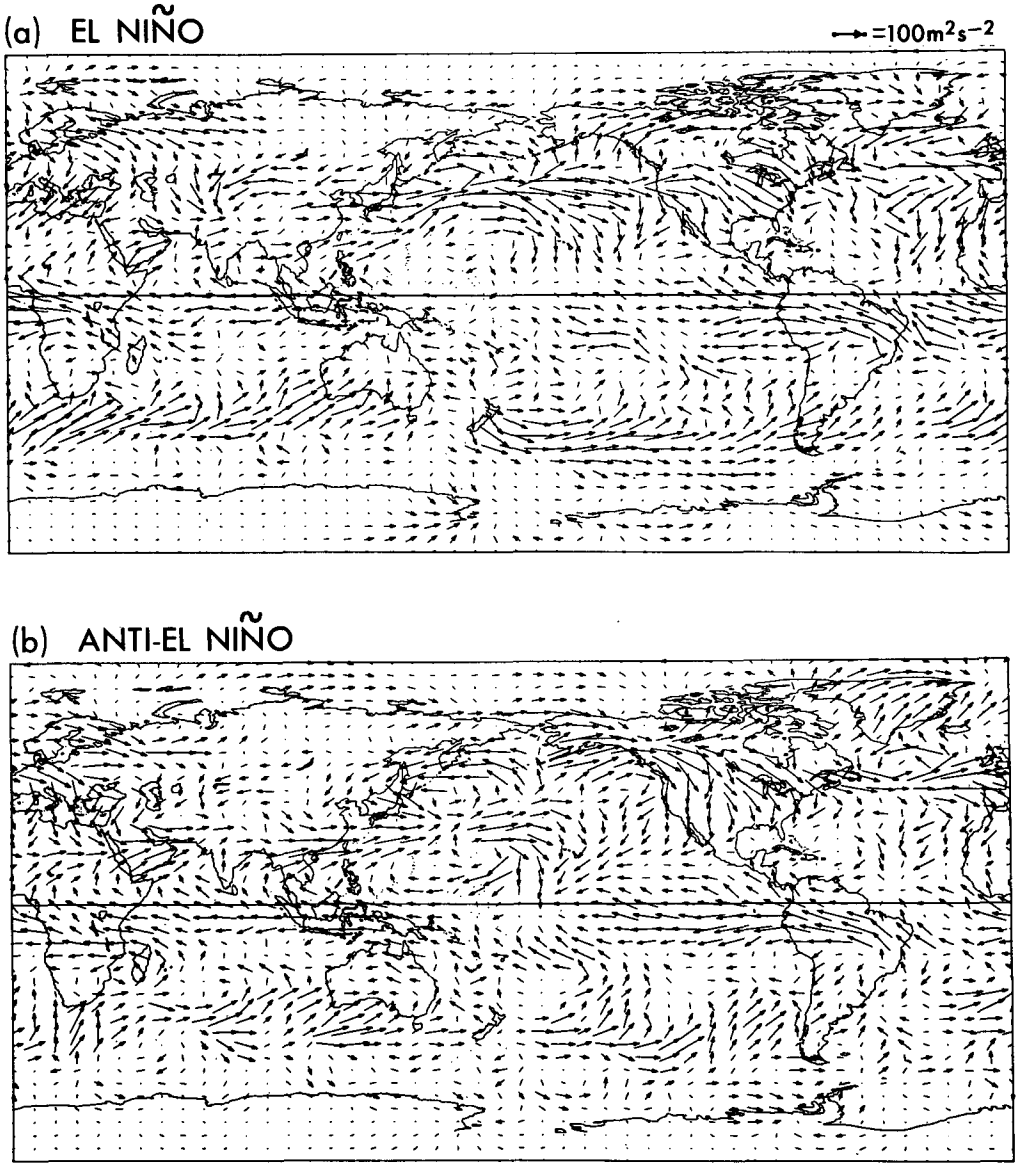

FIG. 10. Plots of the vector $([\overline{v'^2} - \overline{u'^2}]/2, -\overline{u'v'})$ at 200 mb for the GCM (a) El Niño and (b) anti-El Niño composites. A scale for the vector length is included in the upper right-hand corner.

tropospheric eddies are modified by the tropical heating distribution in the GCM. On the one hand, redistribution of the tropical heating directly results in modified upper tropospheric equatorial zonal winds: in El Niño winters, the Walker circulation weakens and there is an easterly zonal wind anomaly in the upper troposphere over the Pacific. The perturbed zonal winds then modify the spectrum of Rossby waves propagating into the tropical Pacific from higher latitudes, as described by Webster and Holton (1982). Stronger easterlies prevent some of these Rossby waves from penetrating as far equatorwards as they normally would; the easterly acceleration associated with the absorption of these waves in low latitudes is displaced polewards as a result, broadening the easterly anomaly and substantially modifying the directly forced extratropical wave train.

The midlatitude storm track transients are modified in a different manner. The equatorwards movement of the eastern half of the Pacific storm track in El Niño winters must be a response to the modified extratropical stationary wave field itself. Since the anomalous midlatitude transients in turn force a substantial part of the anomalous extratropical wave train, the storm track transients must be providing a strong positive feedback.

The zonal asymmetry of the midlatitude transients

is presumably of central importance to this strong feedback. It seems plausible that a modest disturbance from the tropics can more easily displace the downstream tail of an oceanic storm track, where upper level barotropic dispersion dominates, than the upstream end whose position is controlled by the low level baroclinicity. Thus, the influence of the climatological stationary eddies on the tropically forced anomalous wave train, evident in the GCMs analyzed by Geisler et al. (1985), Palmer and Mansfield (1986), and Blackmon et al. (1987), can occur through storm track structure as well as through direct interaction of the mean fields.

A rather complex picture emerges from this analysis of a GCM's response to tropical ocean temperature anomalies. The anomalous upper tropospheric vorticity tendency in low latitudes forces a modest extratropical wave train which is then strengthened by feedback with the storm track eddies. The anomalous low latitude vorticity tendencies are themselves due partly to the anomalous latent heating itself and partly to a redistribution of Rossby wave drag that occurs because the tropical zonal winds are modified by the heating anomalies. The relative importance of the different links in this chain, as well as the importance of nonlinearity in the stationary wave field itself, may be sensitive to the details of the forcing.

Acknowledgments. We would like to thank N. C. Lau for his assistance with the analysis of the GCM data.

APPENDIX

Linear Model Description

The model solves the steady linear primitive equations on the sphere using $\sigma = p/p_s$ as the vertical coordinate. The equations are linearized about a zonally averaged state that can include a mean meridional circulation; however, the mean meridional circulation is set to zero for the calculations in this paper.

In terms of the variables $(U, V) = [u\cos(\theta), v\cos(\theta)]$, the following equations result:

$$\frac{\bar{U}}{a\cos^2\theta}\frac{\partial U'}{\partial\lambda} + \frac{\bar{V}}{a\cos\theta}\frac{\partial U'}{\partial\theta} - \left(2\Omega\sin\theta - \frac{1}{a\cos\theta}\frac{\partial\bar{U}}{\partial\theta}\right)V' + \bar{\dot{\sigma}}\frac{\partial U'}{\partial\sigma} + \dot{\sigma}'\frac{\partial\bar{U}}{\partial\sigma}$$
$$= -\frac{1}{a}\frac{\partial\phi'}{\partial\lambda} - \frac{R\bar{T}}{a}\frac{\partial(\ln p_s)'}{\partial\lambda} - \epsilon U' + \nu\cos\theta\nabla^2\left(\frac{U'}{\cos\theta}\right) + F'_u, \quad \text{(A1)}$$

$$\frac{\bar{U}}{a\cos^2\theta}\frac{\partial V'}{\partial\lambda} + 2\left\{\Omega\sin\theta + \frac{\bar{U}\tan\theta}{a\cos\theta}\right\}U' + \frac{\cos\theta}{a}\frac{\partial}{\partial\theta}\left\{\frac{\bar{V}V'}{\cos^2\theta}\right\} + \bar{\dot{\sigma}}\frac{\partial V'}{\partial\sigma} + \dot{\sigma}'\frac{\partial\bar{V}}{\partial\sigma}$$
$$= -\frac{\cos\theta}{a}\left\{\frac{\partial\phi'}{\partial\theta} + R\bar{T}\frac{\partial(\ln p_s)'}{\partial\theta} + RT'\frac{\partial(\overline{\ln p_s})}{\partial\theta}\right\} - \epsilon V' + \nu\cos\theta\nabla^2\left(\frac{V'}{\cos\theta}\right) + F'_v, \quad \text{(A2)}$$

$$\frac{1}{a\cos\theta}\left\{\frac{\bar{U}}{\cos\theta}\frac{\partial T'}{\partial\lambda} + \bar{V}\frac{\partial T'}{\partial\theta} + V'\frac{\partial\bar{T}}{\partial\theta}\right\} + \bar{\dot{\sigma}}\frac{\partial T'}{\partial\sigma} + \dot{\sigma}'\frac{\partial\bar{T}}{\partial\sigma} = \frac{R\bar{T}}{c_p}\left\{\frac{\dot{\sigma}'}{\sigma} - \frac{\partial\dot{\sigma}'}{\partial\sigma} - \frac{1}{a\cos\theta}\left\{\frac{1}{\cos\theta}\frac{\partial U'}{\partial\lambda} + \frac{\partial V'}{\partial\theta}\right\}\right\}$$
$$+ \frac{RT'}{c_p}\left\{\frac{\bar{\dot{\sigma}}}{\sigma} - \frac{\partial\bar{\dot{\sigma}}}{\partial\sigma} - \frac{1}{a\cos\theta}\frac{\partial\bar{V}}{\partial\theta}\right\} + \frac{\dot{Q}'}{c_p} + \nu\nabla^2 T', \quad \text{(A3)}$$

$$\int_0^1\left[\frac{\bar{U}}{\cos\theta}\frac{\partial(\ln p_s)'}{\partial\lambda} + \bar{V}\frac{\partial(\ln p_s)'}{\partial\theta} + V'\frac{\partial(\overline{\ln p_s})}{\partial\theta} + \frac{1}{\cos\theta}\frac{\partial U'}{\partial\lambda} + \frac{\partial V'}{\partial\theta}\right]d\sigma = 0, \quad \text{(A4)}$$

$$\frac{\partial\phi'}{\partial\sigma} = -\frac{RT'}{\sigma}, \quad \text{(A5)}$$

$$\dot{\sigma}' = -\frac{1}{a\cos\theta}\int_0^\sigma\left[\frac{\bar{U}}{\cos\theta}\frac{\partial(\ln p_s)'}{\partial\lambda} + \bar{V}\frac{\partial(\ln p_s)'}{\partial\theta} + V'\frac{\partial(\overline{\ln p_s})}{\partial\theta} + \frac{1}{\cos\theta}\frac{\partial U'}{\partial\lambda} + \frac{\partial V'}{\partial\theta}\right]d\sigma. \quad \text{(A6)}$$

The overbar denotes the zonal and time mean, the prime denotes the departure from this mean, ϵ is the latitudinally and vertically varying Rayleigh dissipation coefficient, ν is the constant coefficient of horizontal diffusion, $\dot{Q}'$ is the eddy diabatic heating rate per unit mass plus the temperature tendency due to transient eddies, while F'_u and F'_v are the momentum tendencies due to transient eddies. The rest of the notation is standard.

Equations (A1)–(A6) comprise the linear PE model. In this model, the forcing due to diabatic heating and transient eddy fluxes is present explicitly in the terms $\dot{Q}'$, F'_u, and F'_v. The orographic forcing only appears in the lower boundary condition used in the vertical

integration of the hydrostatic equation (A5), i.e., in the value of ϕ' at $\sigma = 1$.

The two-dimensional basic state and the three-dimensional unknown eddy variables are represented in the linear PE model just as in the GFDL GCM except in the meridional direction; the GCM uses a fully spectral while the linear PE model uses a semispectral horizontal representation of the variables. In the linear model, the eddy geopotential, for example, is represented as

$$\phi'(\lambda, \theta, \sigma) = \sum_{m=1}^{15} 2\,\mathrm{Re}\{\hat{\phi}_m(\theta, \sigma)e^{im\lambda}\} \quad \text{(A7)}$$

where $\hat{\phi}_m(\theta, \sigma)$ is the complex amplitude of the mth zonal wavenumber. Each zonal wavenumber can be solved for separately. The resulting set of equations is finite-differenced in the meridional as well as in the vertical directions. Meridional finite-differencing was chosen over spectral decomposition because the sparse matrices that result allow one to consider calculations with high meridional resolution. An exact linearization of the R15 spectral GCM has recently been constructed at GFDL, and a comparison of the two models shows the differences in the solutions to be extremely small.

The discretization in the vertical is performed using nine unevenly spaced full-sigma levels (0.025, 0.095, 0.205, 0.350, 0.515, 0.680, 0.830, 0.940, and 0.990) which are identical to those used in the GCM. All dynamical quantities except the vertical velocity $\dot{\sigma}$ are defined at these sigma levels; $\dot{\sigma}$ is defined at the half-sigma levels located halfway between the adjacent full levels. The vertical advection of any quantity A is written as

$$\left[\dot{\sigma}\frac{\partial A}{\partial \sigma}\right]_k = \dot{\sigma}_{k-1/2}\left\{\frac{A_k - A_{k-1}}{2(\sigma_k - \sigma_{k-1})}\right\} + \dot{\sigma}_{k+1/2}\left\{\frac{A_{k+1} - A_k}{2(\sigma_{k+1} - \sigma_k)}\right\}. \quad \text{(A8)}$$

The top and bottom boundary conditions take the same very simple form in σ-coordinates that they have in the GCM:

$$\dot{\sigma}_{1/2} = \dot{\sigma}_{9\frac{1}{2}} = 0.$$

In the linear model, the vertical integration of the hydrostatic equation is performed, as in the GCM, using the following formula for the layer thickness between two full sigma levels:

$$\phi_k = \phi_{k+1} + T_{k+1}\ln\left(\frac{\sigma_{k+1}}{\sigma_{k+1/2}}\right) + T_k\ln\left(\frac{\sigma_{k+1/2}}{\sigma_k}\right), \quad \text{(A9)}$$

with

$$\phi_9 = \phi_s + T_9\ln\left(\frac{1}{\sigma_9}\right), \quad \text{(A10)}$$

where ϕ_s is the orography.

The equations are discretized in the meridional direction using a regular grid of $N = 101$ points between the two poles ($\Delta\theta = 1.8°$). All variables except the meridional velocity are defined on this grid ($j = 1$ is the South Pole while $j = N$ is the North Pole); V is defined at the $N - 1$ points located midway between these grid points. The meridional advection of any quantity A is defined as

$$\left[\frac{V}{\cos(\theta)}\frac{\partial A}{\partial \theta}\right]_j = \frac{V_{j+1/2}}{2c_{j+1/2}}\left\{\frac{A_{j+1} - A_j}{\Delta\theta}\right\} + \frac{V_{j-1/2}}{2c_{j-1/2}}\left\{\frac{A_j - A_{j-1}}{\Delta\theta}\right\}, \quad \text{(A11)}$$

where

$$c_{j+1/2} = \cos\left(\theta_j \pm \frac{\Delta\theta}{2}\right).$$

An analogous formula is used to compute derivatives at the staggered grid points at which the meridional momentum equation is applied. For the Coriolis force in the zonal (meridional) momentum equation, $V(U)$ is averaged over the two neighboring points.

In order to remain single-valued, all eddy variables including the wavenumber 1 component of $V' = v'\cos(\theta)$ must vanish at both poles. This condition provides the boundary condition for all variables defined at the polar points. As the eddy meridional velocity is defined half a grid distance away from the poles, we set

$$V'_{1/2} = V'_{3/2}/3 \quad V_{100\frac{1}{2}} = V_{99\frac{1}{2}}/3$$

in order that the linearly extrapolated value of V at the poles be zero.

After the finite-differencing, one obtains equations for U', V', T', and $\ln(p_s)'$ that are meridionally coupled across four adjacent grid points (because of the staggered grid) and vertically coupled across all levels (because ϕ' and $\dot{\sigma}'$ are obtained from vertical integrations). Considering U'_j, $V'_{j+1/2}$, and T'_j at all levels plus $\ln(p_s)'_j$ as one unknown vector of length $1 + 3K$, for $j = 2$ to $N - 1$, the problem reduces to solving a block $(N - 2) \times (N - 2)$ matrix equation in which each block is a $(1 + 3K) \times (1 + 3K)$ matrix. The block matrix has four nonzero bands, corresponding to the latitudinal grid points $(j - 1)$, j, $(j + 1)$, and $(j + 2)$; the $(j + 2)$ band is extremely sparsely filled. Since there is one less grid point for V than for the other variables, the last row of the block matrix has elements of dimension only $(1 + 2K) \times (1 + 2K)$. Gaussian elimination is used to generate a block triangular matrix. Complex matrix inversions are performed using the IMSL routines. Once the solution vector is known, ϕ' and $\dot{\sigma}'$ are obtained using (A5) and (A6).

If the advection by the meridional circulation and the diffusion were not included, the system could have been reduced to an equation in one variable, as in Sim-

mons (1982). When either the meridional advection or the diffusion is retained this simplification does not appear possible.

The matrix elements depend on the basic fields as well as on the damping coefficients. A linearized version of a full GCM is sometimes used to determine these elements by repeatedly integrating the model one time step forward using different initial conditions for the eddy fields (e.g., Hoskins and Karoly 1981). We could not use such a procedure for our model because its meridional differencing differs from that of the GCM. The matrix elements were therefore determined analytically. The calculation is entirely straightforward, but the resulting expressions are sufficiently lengthy to preclude their inclusion here. The best check we have of these calculations is that a completely independent, fully spectral linear model produces nearly identical results.

REFERENCES

Blackmon, M. L., G. W. Branstator, G. T. Bates and J. E. Geisler, 1987: An analysis of equatorial Pacific sea surface temperature anomaly experiments in general circulation models with and without mountains. *J. Atmos. Sci.*, **44,** 1828–1844.

Branstator, G., 1985: Analysis of general circulation model sea-surface temperature anomaly simulations using a linear model. Part I: Forced solutions. *J. Atmos. Sci.*, **42,** 2225–2241.

Geisler, J. E., M. L. Blackmon, G. T. Bates and S. Munoz, 1985: Sensitivity of January climate response to the magnitude and position or equatorial Pacific sea surface temperature anomalies. *J. Atmos. Sci.*, **42,** 1037–1049.

Held, I. M., and I.-S. Kang, 1987: Barotropic models of the extratropical response to El Niño. *J. Atmos. Sci.*, **44,** 1433–1452.

Hoskins, B. J., and D. J. Karoly, 1981: The steady linear response of a spherical atmosphere to thermal and orographic forcing. *J. Atmos. Sci.*, **38,** 1179–1196.

——, I. N. James and G. H. White, 1983: The shape, propagation, and mean-flow interaction of large-scale weather systems. *J. Atmos. Sci.*, **40,** 1545–1612.

Kok, C. J., and J. D. Opsteegh, 1985: On the possible causes of anomalies in seasonal mean circulation pattern during the 1982/83 El Nino event. *J. Atmos. Sci.*, **42,** 677–694.

Lau, N.-C., 1985: Modeling the seasonal dependence of the atmospheric response to observed El-Niños in 1962–76. *Mon. Wea. Rev.*, **113,** 1970–1996.

——, 1988: Variability of the observed midlatitude storm tracks in relation to low-frequency changes in the circulation pattern. *J. Atmos. Sci.*, **45,** to appear.

Manabe, S., D. G. Hahn and J. L. Holloway, Jr., 1979: Climate simulations with GFDL spectral models of the atmosphere: Effects of spectral truncation. Report of the JOC Study Conf. on Climate Models: Performance, Intercomparison and Sensitivity Studies, Washington DC, GARP Publ. Ser. No. 22, Vol. 1, 41–94. [NTIS N8027917]

Nigam, S., I. M. Held and S. W. Lyons, 1986: Linear simulation of the stationary eddies in a general circulation model. Part I: The no-mountain model. *J. Atmos. Sci.*, **43,** 2944–2961.

——, —— and ——, 1988: Linear simulation of the stationary eddies in a general circulation model. Part II: The mountain model. *J. Atmos. Sci.*, **45,** 1433–1452.

Palmer, T. N., and D. A. Mansfield, 1986: A study of wintertime circulation anomalies during past El-Niño events, using a high resolution general circulation model. I: Influence of model climatology. *Quart. J. Roy. Meteor. Soc.*, **112,** 613–638.

Plumb, R. A., 1986: Three-dimensional propagation of quasi-geostrophic eddies and its relationship with the eddy forcing of the time mean flow. *J. Atmos. Sci.*, **43,** 1651–1678.

Simmons, A. J., 1982: The Forcing of Stationary Wave Motions by Tropical Diabatic Heating. *Quart. J. Roy. Meteor. Soc.*, **108,** 503–534.

——, J. M. Wallace and G. Branstator, 1983: Barotropic wave propagation and instability, and atmospheric teleconnection patterns. *J. Atmos. Sci.*, **40,** 1363–1392.

Webster, P. J., and J. R. Holton, 1982: Cross-equatorial response to middle-latitude forcing in a zonally varying basic state. *J. Atmos. Sci.*, **39,** 722–733.